Inorganic Chemistry

Article

pubs.acs.org/IC

Synthesis and Spectroscopy of Anionic Cyclometalated Iridium(III)-Dithiolate and -Sulfinates—Effect of Sulfur Dioxygenation on Electronic Structure and Luminescence

Van Ha Nguyen, Hui Qi Chew, Bochao Su, and John H. K. Yip*

Department of Chemistry, National University of Singapore, 3 Science Drive 3, Singapore 117543

Supporting Information

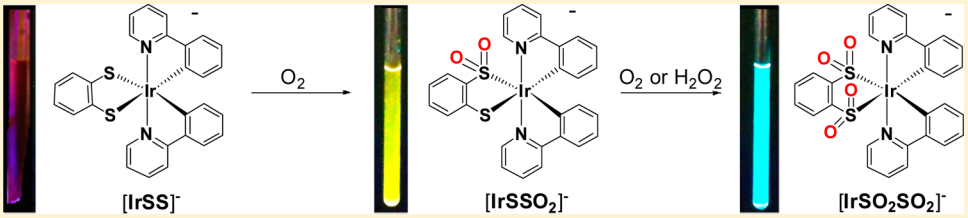

ABSTRACT: A new anionic heteroleptic Ir(III)-dithiolate complex Ir(ppy)$_2$(benzene-1,2-dithiolate) (ppy = 2-phenylpyridine, [**IrSS**]$^-$) undergoes very fast air oxidation to form a monosulfinate complex [**IrSSO$_2$**]$^-$, which can be further dioxygenated by O_2 or H_2O_2 to give a disulfinate complex [**IrSO$_2$SO$_2$**]$^-$, which has been characterized by X-ray crystallography. The dioxygenation is accompanied by changes in the electronic structures of the complexes, leading to blue shift of emission from [**IrSS**]$^-$ (λ_{max} = 665 nm) to [**IrSSO$_2$**]$^-$ (λ_{max} = 556 nm) and to [**IrSO$_2$SO$_2$**]$^-$ (λ_{max} = 460 nm). The molecular and electronic structures of the complexes are probed by DFT calculations. Time-dependent DFT (TD-DFT) calculations show the lowest energy spin-allowed electronic transitions for [**IrSS**]$^-$ and [**IrSSO$_2$**]$^-$ are mainly ligand (3p orbital of S)-to-ligand (π^* orbitals of ppy)-charge-transfer transition, whereas the lowest energy electronic transition in [**IrSO$_2$SO$_2$**]$^-$ is predominantly metal-to-ligand-charge transfer in nature.

INTRODUCTION

Since the early work of Watts' on the photophysics and photochemistry of homoleptic ortho-cyclometalated iridium-(III) complex *fac*-[Ir(ppy)$_3$] (ppy = 2-phenylpyridine),[1a] the numerous derivatives of the complex have emerged into an important class of luminescent molecules[1b−1x] that find applications in OLED,[2] photocatalysis,[2b,3] dye sensitized solar cells,[3c,4] photovoltaics,[5] or phosphorescent bioimaging.[6] The popularity of the molecules arises mainly from the relatively intense emissions, which can be tuned by varying the electronic structures of the ligands or combination of different ligands.[1c−e,2b,i,7] To meet conditions (e.g., sublimability for OLED or water-solubility for bioimaging probes) required for particular applications, most of the complexes are either neutral or cationic. Anionic cyclometalated Ir(III) complexes are not common,[2f,j] and all reported compounds contain π-accepting cyanide or thiocyanate as the auxiliary ligands, that is, [Ir(ppy)$_2$(CN)$_2$]$^-$ and [Ir(ppy)$_2$(NCS)$_2$]$^-$.[2f]

Metal−thiolates is an important class of molecules because of their biological relevance,[8] reactivity (e.g., oxygenation[9] and nucleophilic substitution[10]) or physical properties (e.g., photo-luminescence[11]), and most of all, investigation of the electronic structures of metal−thiolates led to deeper understanding of the multifaceted metal−sulfur bond.[12] Dithiolates are strong σ- and π-donors with free lone pairs that can take part in electronic transitions and reactions with electrophiles and oxidants. In this paper, we report the synthesis of [Ir-(ppy)$_2$(benzene-1,2-dithiolate)]$^-$ ([**IrSS**]$^-$) (Scheme 1). To the best of our knowledge no *anionic* Ir(ppy)$_2$-dithiolate complex has ever been reported, and only neutral sulfur-ligated complexes [Ir(ppy)$_2$(S$_2$C-NMe$_2$)], [Ir(ppy)$_2$(S$_2$COMe)],[13] [Ir-(ppy)$_2$(S$_2$P(OMe)$_2$)],[14] and [Ir(ppy)$_2$(2-pyridinethiolate)][15] are known.

Metal−thiolates have rich redox chemistry. Darensbourg showed oxygenation of M−N$_2$S$_2$ (M = Ni^{2+} or Pd^{2+}) complexes led to formation of sulfenato (M−N$_2$SS=O) and suflinato (M−N$_2$SSO$_2$ and M−N$_2$SO$_2$SO$_2$) complexes.[9d,16] Some d^6 Fe(II)- and Ru(II)-thiolate complexes display similar oxygenations, which are related to mechanisms of nitrile hydratase[17] and thiocyanate hydrolase.[9b] Lever et al. showed that the complex [Ru(2,2′-bipyridine)$_2$(benzene-1,2-dithiolate)] (**RuSS**), which is an isoelectronic analog of [**IrSS**]$^-$, undergoes dioxygenation to form **RuSSO$_2$** and **RuSO$_2$SO$_2$**.[18] The dioxygenation diminishes the ligand(3p of S)-to-ligand(π^* of 2,2′-bipyridine)-charge-transfer (LLCT) character and increases the metal-to-ligand(π^* of 2,2′-bipyridine)-charge-transfer (MLCT) character in the lowest excited state. In view of the fact that oxidation of sulfur-containing amino acid cysteine is involved in biological sensing for reactive oxygen species (ROS),[19] we envision that coupling a luminescent Ir(ppy)$_2^+$ with the redox-active dithiolate will give rise to a complex

Received: June 3, 2014
Published: August 27, 2014

   dx.doi.org/10.1021/ic501278n | *Inorg. Chem.* 2014, 53, 9739−9750

Scheme 1

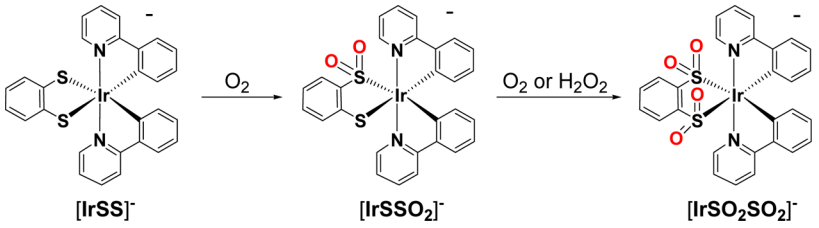

responsive to oxygen or ROS by emitting different colors. Our results show that $[\mathbf{IrSS}]^-$ ion is extremely reactive toward oxygen and produces mono- and disulfinato complexes $[\mathbf{IrSSO_2}]^-$ and $[\mathbf{IrSO_2SO_2}]^-$ (Scheme 1). Unlike the ruthenium analogs, the iridium complexes are luminescent. The oxidation is accompanied by pronounced change in UV–vis absorption and emission due to changes in the electronic structures of the complexes, which have been probed by DFT calculations.

EXPERIMENTAL SECTION

General Methods. All syntheses were carried out in an Ar atmosphere. All the solvents used for syntheses and spectroscopic measurements were purified according to the literature procedures.[20] $Ir_2(ppy)_4(\mu\text{-}Cl)_2$ was prepared according to a reported method.[1] Silver trifluoromethanesulfonate (AgOTf), ^{n}Bu$_4$NCl, Ph$_4$PCl, aqueous solution of H_2O_2 (30%), and benzene-1,2-dithiol were obtained from Aldrich and used without prior purification.

Physical Methods. The UV–vis absorption and emission spectra of the compounds were recorded on a Shimadzu UV-2401PC spectrophotometer and a Horiba FluoroMax-4 fluorescence spectrophotometer, respectively. Emission lifetimes were measured on a Horiba Jobin-Yvon Fluorolog FL-1057 instrument, and 9,10-diphenylanthracene was used as a standard for quantum yield measurements. The solutions for emission spectral, lifetime, and quantum yield measurements were degassed by five freeze–pump–thaw cycles. ^{1}H NMR spectra were obtained on a Bruker Avance 500 spectrometer. All chemical shifts are quoted relative to SiMe$_4$. Electrospray ionization mass spectra (ESI-MS) were obtained using a Finnigan LCQ spectrometer. Isotope distributions were simulated by the Isotope Viewer utility in the Xcalibur (Thermo Scientific) software package. Infrared spectra (KBr pellets) were recorded by a Bruker Alpha spectrometer. Elemental analyses were carried out at Elemental Analysis Laboratory, Department of Chemistry, National University of Singapore.

^{n}Bu$_4$N[Ir(ppy)$_2$(Benzene-1,2-dithiolate)] (^{n}Bu$_4$N[IrSS]). $Ir_2(ppy)_4(\mu\text{-}Cl)_2$ (90 mg, 0.08 mmol) and AgOTf (48 mg, 0.19 mmol) were mixed in 20 mL of acetonitrile (CH_3CN) under argon for 2 h. The resulting solution was filtered and transferred to another Schlenk flask containing benzene-1,2-dithiol (26 mg, 0.18 mmol) and NaOH (22 mg, 0.55 mmol) in 10 mL of methanol (CH_3OH). The mixture was then stirred overnight under argon, and a deep red solution resulted. The solution was concentrated to 5 mL, and ^{n}Bu$_4$NCl (233 mg, 0.84 mmol) in degassed water (50 mL) was added to precipitate the complex as red solids. Solvent was decanted, and the solids were washed several times with degassed water and water/methanol (1/1) mixture before filtration. The product was further purified by diffusing diethyl ether into a MeCN solution of the compound. Yield: 65 mg, 44%. Anal. Calcd (%) for ^{n}Bu$_4$N[**IrSS**] ($C_{44}H_{56}IrN_3S_2$): C, 59.83; H, 6.39; N, 4.76. Found: C, 59.71; H, 6.25; N, 4.70. ^{1}H NMR (500 MHz, CD_3CN) δ 9.87 (dd, $^3J_{H2-H1}$ = 5.9 Hz, $^4J_{H3-H1}$ = 1.6 Hz, 1H, H$_1$), 7.88 (d, $^3J_{H3-H4}$ = 7.7 Hz, 1H, H$_4$), 7.67 (dt, $^3J_{H2/H4-H3}$ = 7.7 Hz, $^4J_{H1-H3}$ = 1.6 Hz, 1H, H$_3$), 7.62 (dd, $^3J_{H6-H5}$ = 7.5 Hz, $^4J_{H7-H5}$ = 1.2 Hz, 1H, H$_5$), 7.04–7.09 (2H, H$_{2,9}$), 6.75 (dt, $^3J_{H5/H7-H6}$ = 7.5 Hz, $^4J_{H8-H6}$ = 1.2 Hz, 1H, H$_6$), 6.64 (dt, $^3J_{H8/H6-H7}$ = 7.5 Hz, $^4J_{H5-H7}$ = 1.2 Hz, 1H, H$_7$), 6.33–6.37 (2H, H$_{10,8}$), 3.03–3.06 (m, 4H, H$_{NBu}$), 1.56–1.59 (m, 4H, H$_{NBu}$), 1.31–1.36 (m, 4H, H$_{NBu}$), 0.96 (t, $^3J_{H-H}$ = 7.3 Hz, 6H, H$_{NBu}$). ESI-MS: m/z 641.04 [**IrSS**]$^-$.

^{n}Bu$_4$N[Ir(ppy)$_2$(Benzene-1-sulfinate-2-thiolate)] (^{n}Bu$_4$N[IrSSO$_2$]). Na[**IrSS**] was prepared in situ by reacting $Ir_2(ppy)_4(\mu\text{-}Cl)_2$ (110 mg, 0.10 mmol), AgOTf (58 mg, 0.23 mmol), benzene-1,2-dithiol (32 mg, 0.23 mmol), and NaOH (27 mg, 0.68 mmol) in CH_3CN/CH_3OH mixture. To the deep red solution, air was injected in 30 mL portions, while the formation of $[\mathbf{IrSSO_2}]^-$ was monitored by ESI-MS. Conversion of $[\mathbf{IrSS}]^-$ to $[\mathbf{IrSSO_2}]^-$ was completed in 12 h after 150 mL of air was admitted. It was accompanied by color change from red to orange and finally to yellow. Addition of ^{n}Bu$_4$NCl (285 mg, 1.03 mmol) in 30 mL of degassed water to the yellow solution precipitated the product as yellow solids, which was washed successively with water and water/methanol (1/1) mixture and dried in vacuum. The compound was purified by diffusing diethyl ether into its CH_3CN solution. Yield: 97 mg, 53%. Anal. Calcd (%) for ^{n}Bu$_4$N[**IrSSO$_2$**] ($C_{44}H_{56}IrN_3S_2O_2$): C, 57.74; H, 6.17; N, 4.59. Found: C, 57.39; H, 6.26; N, 4.70. ^{1}H NMR (500 MHz, CD_3CN) δ 10.22 (dd, $^3J_{H2-H1(H2'-H1')}$ = 5.9 Hz, $^4J_{H3-H1(H3'-H1')}$ = 0.9 Hz, 1H, H$_{1(1')}$), 9.62 (dd, $^3J_{H2'-H1'(H2-H1)}$ = 5.8 Hz, $^4J_{H3'-H1'(H3-H1)}$ = 0.9 Hz, 1H, H$_{1'(1)}$), 7.91–7.94 (2H, H$_{4,4'}$), 7.73–7.79 (2H, H$_{3',3}$), 7.67 (dd, $^3J_{H6'-H5'(H6-H5)}$ = 7.7 Hz, $^4J_{H7'-H5'(H7-H5)}$ = 1.2 Hz, 1H, H$_{5'}$), 7.64 (dd, $^3J_{H6-H5(H6'-H5')}$ = 7.4 Hz, $^4J_{H7-H5(H7'-H5')}$ = 1.2 Hz, 1H, H$_5$), 7.25–7.28 (2H, H$_{9,12}$), 7.13 (ddd, $^3J_{H3-H2(H3'-H2')}$ = 7.4 Hz, $^3J_{H1-H2(H1'-H2')}$ = 5.9, $^4J_{H4-H2(H4'-H2')}$ = 1.5 Hz, 1H, H$_{2(2')}$), 7.09 (ddd, $^3J_{H3'-H2'(H3-H2)}$ = 7.3 Hz, $^3J_{H1'-H2'(H1-H2)}$ = 5.8, $^4J_{H4'-H2'(H4-H2)}$ = 1.4 Hz, 1H, H$_{2'(2)}$), 6.84–6.90 (2H, H$_{10,6'(6)}$), 6.82 (dt, $^3J_{H7/H5-H6(H7'/H5'-H6')}$ = 7.4 Hz, $^4J_{H8-H6(H8'-H6')}$ = 1.2 Hz, 1H, H$_{6(6')}$), 6.72–6.75 (2H, H$_{11,7'(7)}$), 6.68 (dt, $^3J_{H6/H8-H7(H6'/H8'-H7')}$ = 7.4 Hz, $^4J_{H5-H7(H5'-H7')}$ = 1.2 Hz, 1H, H$_{7(7')}$), 6.40 (dd, $^3J_{H7'-H8'(H7-H8)}$ = 7.5 Hz, $^4J_{H6'-H8'(H6-H8)}$ = 1.0 Hz, 1H, H$_{8'(8)}$), 6.19 (dd, $^3J_{H7-H8(H7'-H8')}$ = 7.4 Hz, $^4J_{H6-H8(H6'-H8')}$ = 1.2 Hz, 1H, H$_{8(8')}$), 3.05–3.08 (m, 8H, H$_{NBu}$), 1.55–1.62 (m, 8H, H$_{NBu}$), 1.31–1.36 (m, 8H, H$_{NBu}$), 0.96 (t, $^3J_{H-H}$ = 7.3 Hz, 12H, H$_{NBu}$). ESI-MS: m/z 673.1 [**IrSSO$_2$**]$^-$.

^{n}NBu$_4$[Ir(ppy)$_2$(Benzene-1,2-disulfinate)] (^{n}Bu$_4$N[IrSO$_2$SO$_2$]). Na[**IrSS**] was prepared in situ by reacting $Ir_2(ppy)_4(\mu\text{-}Cl)_2$ (110 mg, 0.10 mmol), AgOTf (58 mg, 0.23 mmol), benzene-1,2-dithiol (32 mg, 0.23 mmol), and NaOH (27 mg, 0.68 mmol) in CH_3CN/CH_3OH mixture. To the solution of the complex was added excess aqueous solution of hydrogen peroxide (30%, 0.5 mL, 5 mmol). The resulting pale yellow solution was dried under vacuum, and the residue was dissolved in a minimum amount of CH_3CN and transferred to a solution of ^{n}Bu$_4$NCl (285 mg, 1.03 mmol) in 50 mL of water to precipitate the compound. The precipitates were isolated by centrifuging and washed with water/methanol mixture. Yield: 126 mg, 67%. Anal. Calcd (%) for ^{n}Bu$_4$N[**IrSO$_2$SO$_2$**] ($C_{44}H_{56}IrN_3S_2O_4$): C, 55.79; H, 5.96; N, 4.44. Found: C, 55.43; H, 6.07; N, 4.50. ^{1}H NMR (500 MHz, CD_3CN) δ 9.90 (dd, $^3J_{H2-H1}$ = 6.0 Hz, $^4J_{H3-H1}$ = 1.5 Hz, 1H, H$_1$), 7.98 (dd, $^3J_{H3-H4}$ = 7.8 Hz, $^4J_{H2-H4}$ = 1.5 Hz, 1H, H$_4$), 7.84 (dt, $^3J_{H2/H4-H3}$ = 7.8 Hz, $^4J_{H1-H3}$ = 1.5 Hz, 1H, H$_3$), 7.67–7.70 (2H, H$_{9,5}$), 7.41–7.43 (m, 1H, H$_{10}$), 7.15 (ddd, $^3J_{H1-H2}$ = 6.0 Hz, $^3J_{H3-H2}$ = 7.8 Hz, $^4J_{H4-H2}$ = 1.5 Hz, 1H, H$_2$), 6.91 (dt, $^3J_{H5/H7-H6}$ = 7.4 Hz, $^4J_{H8-H6}$ = 1.3 Hz, 1H, H$_6$), 6.76 (dt, $^3J_{H6/H8-H7}$ = 7.4 Hz, $^4J_{H5-H7}$ = 1.3 Hz, 1H, H$_7$), 6.27 (dd, $^3J_{H7-H8}$ = 7.4 Hz, $^4J_{H6-H8}$ = 1.3 Hz, 1H, H$_8$), 3.05–3.08 (m, 4H, H$_{NBu}$), 1.58–1.61 (m, 4H, H$_{NBu}$), 1.32–1.37 (m, 4H, H$_{NBu}$), 0.97 (t, $^3J_{H-H}$ = 7.3 Hz, 6H, H$_{NBu}$). ESI-MS: m/z 705.02 [**IrSO$_2$SO$_2$**]$^-$. Addition of excess Ph$_4$PCl to a concentrated

dx.doi.org/10.1021/ic501278n | Inorg. Chem. 2014, 53, 9739–9750

Table 1. Crystal Data for $Ph_4P[IrSO_2SO_2]$

complex	$Ph_4P[\mathbf{IrSO_2SO_2}]$
empirical formula	$C_{52}H_{40}IrN_2O_4PS_2{\cdot}0.55Et_2O{\cdot}0.45MeOH{\cdot}0.9H_2O$
formula weight	1109.18
crystal system	orthorhombic
space group	$P2_12_12_1$
unit cell dimensions	a = 9.684(9), b = 17.926(17), c = 27.04(3) Å
	$\alpha = \beta = \gamma = 90°$
volume (Å^3)	4695(8)
Z	4
density (calculated, g cm^{-3})	1.569
absorption coefficient (mm^{-1})	3.022
F(000)	2218
crystal size (mm^3)	0.46 × 0.16 × 0.04
θ range for data collection (deg)	1.36−25.00
index ranges	$-11 \le h \le 11$, $-17 \le k \le 21$, $-32 \le l \le 30$
reflections collected	28 499
independent reflections (R(int))	8281 (0.0725)
max. and min transmission	0.7456 and 0.5627
data/restraints/parameters	8281/53/641
final R indices[a] [I > 2sigma(I)]	
$R1$	0.0423
$wR2$	0.1034
goodness-of-fit (GOF)[b]	1.123
largest diff. peak and hole (e Å^{-3})	1.359 and −1.841

[a] $R1 = (||F_o| - |F_c||)/(|F_o|)$; $wR2 = [w(F_o^2 - F_c^2)/w(Fo^4)]^{1/2}$; [b] $GOF = [(w(F_o^2 - F_c^2)^2/(n-p)]^{1/2}$. For crystal determination, scan type and wavelength of radiation used is ω and 0.710 73 Å, respectively.

solution of ^{n}Bu$_4$N[**IrSO$_2$SO$_2$**] gave $Ph_4P[\mathbf{IrSO_2SO_2}]$, whose crystals were obtained from vapor diffusion of ether into a methanol solution of the compounds and were characterized by X-ray diffraction.

X-ray Crystallography. Single-crystal X-ray diffraction was carried out on a Bruker AXS SMART CCD three-circle diffractometer with a sealed tube at 223 K using graphite-monochromated Mo Kα radiation (λ = 0.710 73 Å). The software used was as follows: SMART[21] for collecting frames of data, indexing reflections, and determining lattice parameters; SAINT[21a] for integration of intensity of reflections and scaling; SADABS[21b] for empirical absorption correction; SHELXTL[22] for space group determination, structure solution, and least-squares refinements on $|F|^2$. Anisotropic thermal parameters were refined for the rest of the non-hydrogen atoms. The hydrogen atoms were placed in their ideal positions. An unit cell contains one $[\mathbf{IrSO_2SO_2}]^-$ anion and one Ph_4P^+ cation. There were residual electron densities that were assigned to methanol (occupancy = 0.45), H_2O (occupancy = 0.9), and diethyl ether (occupancy = 0.55). Crystal data and experimental details are summarized in Table 1.

Computational Details. The gas-phase ground state geometries of all complexes in were optimized by the DFT method using the Perdew−Wang gradient-corrected correlation functional (B3PW91).[23] The 6-31G(d) basis set was used for all atoms, except iridium, where Stuttgart−Dresden (SDD)[24] relativistic effective core potential and an associated basis set was employed. The unrestricted formalism (UB3PW91) was used with the same basis sets for the optimization of the lowest-lying triplet states. Frequency calculation was performed for all optimized geometry to ensure that the stationary point was minimum. Vibrational spectrum was generated from frequency calculation and was plotted with half-width at half height of 4 cm^{-1}. A scaling of 0.97 was used as it gives good agreement between experimental and theoretical spectra. Single point and time-dependent (TD-DFT) calculation were performed at the same functional and basis sets with solvent effect of acetonitrile (PCM model)[25] incorporated. Emission energy was estimated using ΔSCF approach by taking the difference between energy of the triplet excited state and the ground singlet state at the excited state optimized geometry. TD-DFT triplet excitation using triplet excited state optimized geometry was also calculated for comparison. All DFT calculation was performed using Gaussian 09 software package (Revision A.02).[26] Molecular orbital compositions in term of fragmental contributions were analyzed with *AOMix* program.[27] Other functional/basis set combinations including B3LYP/(6-31G(d) + LANL2DZ), B3LYP/(6-31G(d) + SDD), and B3PW91/(6-31G(d) + LANL2DZ) were used to calculate the molecular, electronic structures, and absorption spectra of the complexes. B3PW91/(6-31G(d)+SDD) combination gives the best agreement with the crystal structure of $[\mathbf{IrSO_2SO_2}]^-$ and electronic spectra of the complexes and thus is used for discussion. However, the results of all the methods are similar, especially the nature of the frontier orbitals and major electronic transitions.

RESULTS AND DISCUSSION

Synthesis and Structures. The complex [**IrSS**]$^-$ was synthesized by reacting *cis*-$[Ir(ppy)_2(MeCN)_2]^+$ and benzene-1,2-dithiolate generated *in situ*. Deep red solids and CH_3CN solution of ^{n}Bu$_4$N[**IrSS**] are extremely air-sensitive, suggesting that the sulfur atoms are electron-rich. It is reasonable considering the formal negative charge of the complex. In addition, the lone pairs of the S atoms can be destabilized by antibonding interactions between the 3p orbitals and the filled

Scheme 2

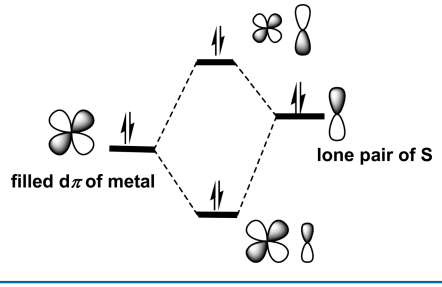

dx.doi.org/10.1021/ic501278n | Inorg. Chem. 2014, 53, 9739−9750

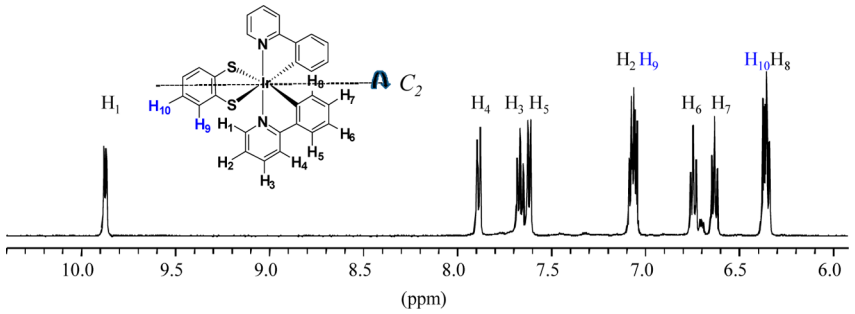

Figure 1. ^{1}H NMR spectrum of ^{n}Bu$_4$N[**IrSS**] in CD$_3$CN solution.

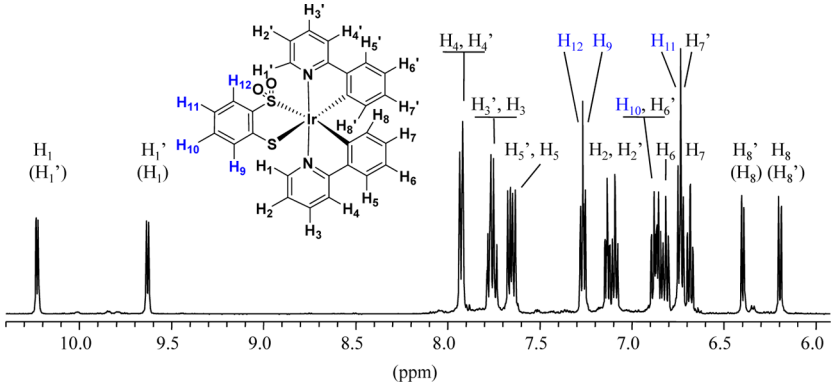

Figure 2. ^{1}H NMR spectrum of ^{n}Bu$_4$N[**IrSSO$_2$**] in CD$_3$CN solution.

Scheme 3

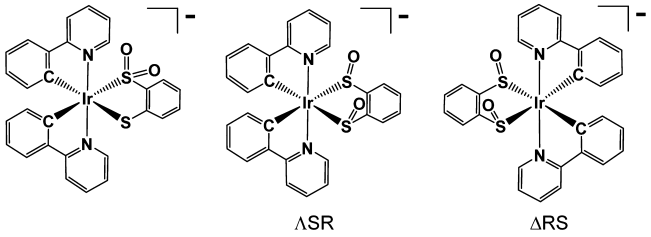

t_{2g} orbitals of the metal, the so-called the filled dπ−pπ interactions (Scheme 2).[9d,10b,28]

^{1}H NMR spectrum (Figure 1) shows only one set of eight aromatic signals for ppy (δ 9.87, 7.88, 7.67, 7.07, 6.75, 6.72, 6.64, and 6.34) and two doublets for benzene-1,2-dithiolate (δ 6.37 and 7.08), indicating the two ppy ligands are equivalent and there is a C_2 symmetry of the molecule whose C_2 axis bisects the dithiolate. Assignment of the signals was made with the aid of two-dimensional correlation spectroscopy (2D-COSY) (Supporting Information, Figure S1).

ESI-MS of the complex shows a prominent parental peak (m/z = 641.04) for [**IrSS**]$^-$ which shows an isotopic distribution essentially identical with the ones calculated according to the proposed molecular formula, m/z = 641.07 (Supporting Information, Figure S2). Exposing solution of [**IrSS**]$^-$ to air in darkness causes a spontaneous color change from red to yellow. The major product shows a molecular ion peak at m/z = 673.06 in its ESI-MS (Supporting Information, Figure S3), indicating the reaction is a dioxygenation in which two oxygen atoms are added to [**IrSS**]$^-$ (m/z = 641.07). The other product is confirmed to be [**IrSO$_2$SO$_2$**]$^-$. Prolonged air

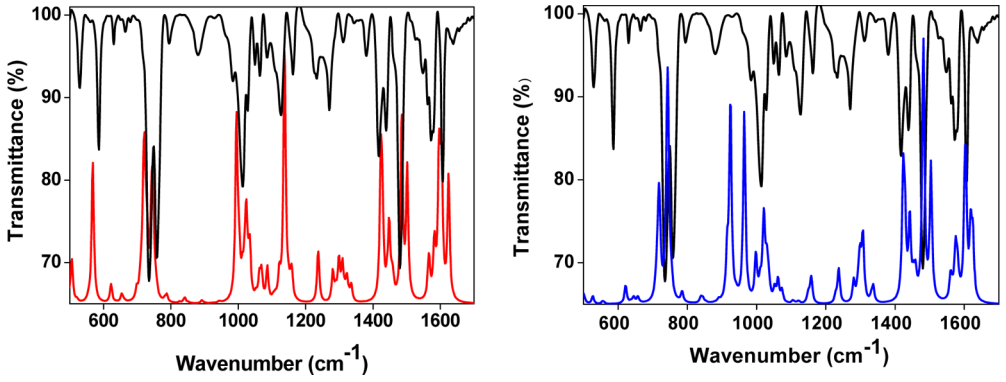

Figure 3. Experimental (black) and DFT-calculated IR spectra for the dioxygenation product (black), [**IrSSO$_2$**]$^-$ (left, red), and [**IrSOSO**]$^-$ (right, blue).

dx.doi.org/10.1021/ic501278n | Inorg. Chem. 2014, 53, 9739−9750

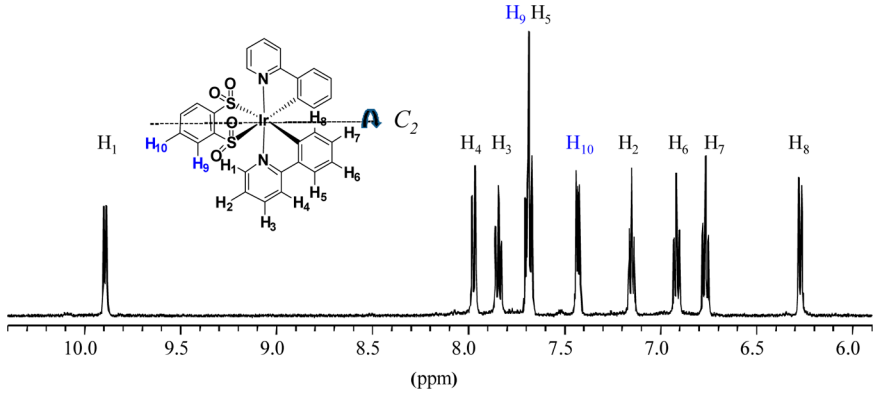

Figure 4. ^{1}H NMR spectrum of ^{n}Bu$_4$N[**IrSO$_2$SO$_2$**] in CD_3CN solution.

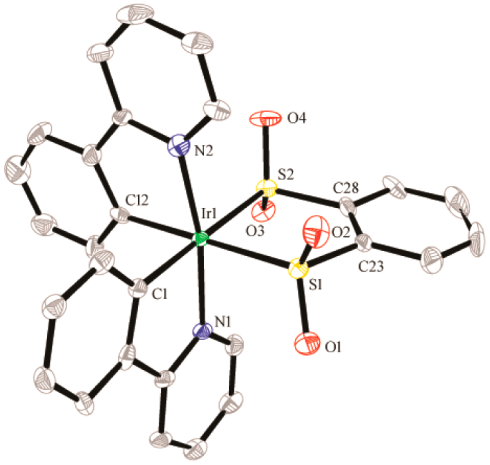

Figure 5. ORTEP plot of [**IrSO$_2$SO$_2$**]$^-$ (thermal ellipsoids drawn at 50% probability level). H atoms, Ph_4P^+ cation, and solvent molecules are omitted for clarity. Color Scheme: Ir (green), S (yellow), O (red), N (blue), C (gray).

Table 2. Selected Bond Lengths (Å) and Angles (deg) of Ph$_4$P[IrSO$_2$SO$_2$]

Ir(1)−C(1)	2.049(9)	C(1)−Ir(1)−N(1)	80.1(3)
Ir(1)−C(12)	2.058(9)	C(12)−Ir(1)−N(2)	79.4(3)
Ir(1)−N(1)	2.081(7)	S(1)−Ir(1)−S(2)	87.56(10)
Ir(1)−N(2)	2.059(7)	C(1)−Ir(1)−S(2)	178.9(2)
Ir(1)−S(1)	2.352(3)	C(12)−Ir(1)−S(1)	179.8(3)
Ir(1)−S(2)	2.348(2)	N(1)−Ir(1)−N(2)	169.4(3)
S(1)−C(23)	1.807(8)	Ir(1)−S(1)−C(23)	104.9(3)
S(2)−C(28)	1.811(8)	Ir(1)−S(2)−C(28)	105.2(3)
S(1)−O(1)	1.477(6)	O(1)−S(1)−O(2)	111.7 (4)
S(1)−O(2)	1.467(6)	O(3)−S(2)−O(4)	112.1(4)
S(2)−O(3)	1.471(6)		
S(2)−O(4)	1.485(6)		

exposure leads to conversion of the major product to [**IrSO$_2$SO$_2$**]$^-$.

^{1}H NMR spectrum of the major product (Figure 2) is more complicated than that of ^{n}Bu$_4$N[**IrSS**], showing 20 signals in the aromatic region. The signals, assigned with the aid of the 2D-COSY spectrum of the compound (Supporting Information, Figure S4), can be grouped into two sets of eight signals for ppy and two sets of two signals of benzenethiolate. This observation indicates dioxygenation leads to a lost of C_2 symmetry and accordingly the dioxygenation product could be a thiolate−sulfinate complex or a disulfenate complex [**IrSOSO**]$^-$ (Scheme 3). There are six optical isomers for the disulfenate complex but only the two enantiomers ΛSR and ΔRS are deprived of any C_2 axis.

Lever et al. demonstrated that S═O bond stretching frequencies can be used to distinguished **RuSSO$_2$** and **RuSOSO**.[18] Figure 3 shows the experimental IR spectrum of the dioxygenation product and the DFT calculated spectra of [**IrSSO$_2$**]$^-$ and [**IrSOSO**]$^-$. The DFT-calculated IR spectrum of [**IrSSO$_2$**]$^-$ closely resembles the experimental spectrum. Most importantly, the calculation predicts stretching frequencies of S═O bonds (symmetric mode at 994 cm^{-1} and asymmetric mode at 1136 cm^{-1}) and Ir−S(O_2) bonds (568 cm^{-1}) close to the experimental values (1013, 1126, and 586 cm^{-1}, respectively). On the contrary, the calculated IR spectrum of [**IrSOSO**]$^-$ fails to reproduce the salient features of the experimental spectrum and it gives S═O stretching frequencies (924 and 964 cm^{-1}) significantly lower than the experimental values. Note that the dioxygenation product displays S═O stretching frequencies (1013 and 1126 cm^{-1}) close to those observed (1014 and 1149 cm^{-1}) in the IR spectra of [$IrSO_2SO_2$]$^-$ (vide infra), **RuSSO$_2$** (983 and 1105 cm^{-1}) and **RuSO$_2$SO$_2$** (989 and 1119 cm^{-1}).[18] It is therefore reasonable to formulate the dioxygenation product as the thiolate−sulfinate [**IrSSO$_2$**]$^-$ complex.

The complex [**IrSO$_2$SO$_2$**]$^-$ can be produced slowly by air oxidation of [**IrSS**]$^-$. For example, a 5 mL portion of 1 mM solution of ^{n}Bu$_4$N[**IrSS**]$^-$ takes 7 h to be completely oxidized by air to ^{n}Bu$_4$N[**IrSO$_2$SO$_2$**]. But addition of excess H_2O_2 solution (30%) can complete the oxidation in less than 5 min. The attenuated reactivity of [**IrSSO$_2$**]$^-$ toward the second dioxygenation is due to lower energy of the lone pair of the remaining thiolate S atom as shown by the DFT calculation (vide infra). It can be accounted that the first dioxygenation leads to a poor electron-donating sulfinates, and as a result, the iridium ion in [**IrSSO$_2$**]$^-$ becomes more electron withdrawing, leading to a decrease in the energy of the lone pairs of the remaining thiolate.

^{1}H NMR spectrum of [**IrSO$_2$SO$_2$**]$^-$ (Figure 4) regains the simplicity of the [**IrSS**]$^-$ spectrum, showing only ten signals of which eight belong to the two ppy ligands and two belong to the benzenethiolate, indicating the second dioxygenation restores the C_2 symmetry of the molecule which consists of two sulfinates (see Supporting Information for the 2D-COSY (Figure S5) and ESI-MS (Figure S6)).

IR spectrum of the complex shows ν(S═O) bands at 1014 and 1149 cm^{-1}, which are in the range of reported S═O

dx.doi.org/10.1021/ic501278n | Inorg. Chem. 2014, 53, 9739−9750

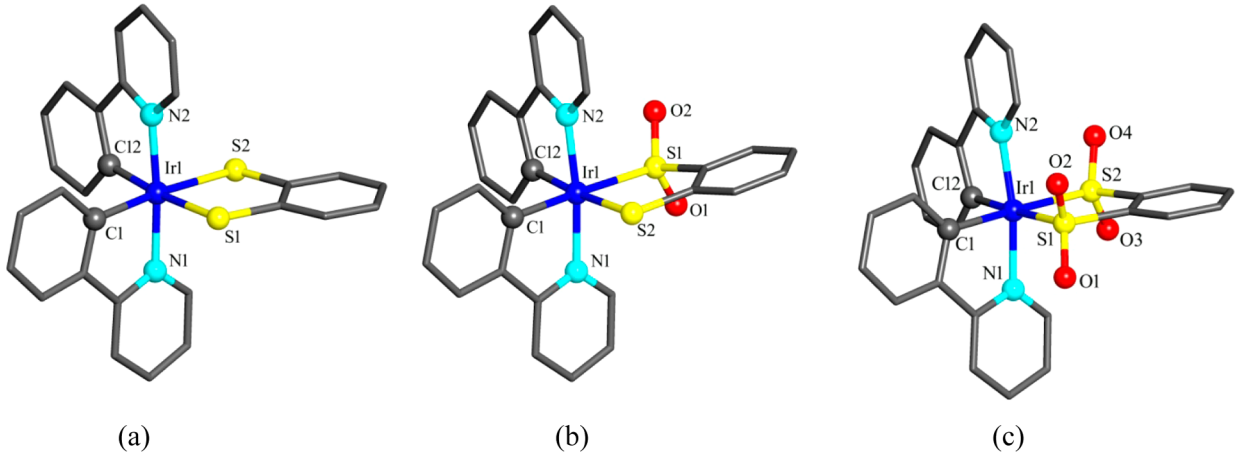

Figure 6. B3PW91/(6-31G(d) + SDD) optimized structures for (a) $[\mathbf{IrSS}]^-$, (b) $[\mathbf{IrSSO_2}]^-$, and (c) $[\mathbf{IrSO_2SO_2}]^-$.

Table 3. Selected Bond Lengths (Å) and Bond Angles (deg) in the Optimized Structures of $[\mathbf{IrSS}]^-$, $[\mathbf{IrSSO_2}]^-$, and $[\mathbf{IrSO_2SO_2}]^-$

	$[\mathbf{IrSS}]^-$	$[\mathbf{IrSSO_2}]^-$	$[\mathbf{IrSO_2SO_2}]^-$	$[\mathbf{IrSO_2SO_2}]^{-a}$
Ir(1)−N(1)	2.062	2.070	2.077	2.081(7)
Ir(1)−N(2)	2.062	2.068	2.077	2.059(7)
Ir(1)−C(1)	2.032	2.043	2.045	2.049(9)
Ir(1)−C(12)	2.032	2.033	2.045	2.058(9)
Ir(1)−S(1)	2.457	2.406	2.405	2.352(3)
Ir(1)−S(2)	2.457	2.468	2.405	2.348(2)
S(1)−O(1)	*b*	1.509	1.495	1.477(6)
S(1)−O(2)	*b*	1.498	1.506	1.467(6)
S(2)−O(3)	*b*	*b*	1.506	1.471(6)
S(2)−O(4)	*b*	*b*	1.495	1.485(6)
N(1)−Ir(1)−N(2)	174.86	172.84	171.16	169.4(3)
N(1)−Ir(1)−C(1)	79.65	79.50	79.58	80.1(3)
N(2)−Ir(1)−C(12)	79.65	79.73	79.58	79.4(3)
S(1)−Ir(1)−S(2)	85.79	86.10	87.23	87.56(10)
O(1)−S(1)−O(2)	*b*	113.41	113.90	111.7(4)
O(3)−S(2)−O(4)	*b*	*b*	113.90	112.1(4)

[a]Experimental data. [b]Not applicable.

stretching frequency of metal-disulfinates (989−1202 cm^{-1}).[16c,18] Pale yellow crystals of $Ph_4P[\mathbf{IrSO_2SO_2}]$, obtained from cation metathesis of the $^nBu_4N$ salt, shows an anionic six-coordinate Ir complex in approximate C_2 symmetry (Figure 5 and Table 2 for selected bond lengths and angles). The two ppy ligands and the benzene-1,2-disulfinate anion form three five-membered chelate rings with the central Ir ion. The Ir−C bond distances (2.049(9) and 2.058(9) Å) are longer than those in the heteroleptic complexes $Ir(ppy)_2(acac)$[2e] (2.003(9) Å) and $[Ir(ppy)_2(en)]ClO_4$[29] (2.015(6) and 2.015(4) Å), suggesting the disulfinate exerts a stronger *trans*-influence than the ligands acetylacetonate (acac) and ethylenediamine (en). The SO_2SO_2-phenyl ring is slightly canted from the Ir−S_2 plane, forming a dihedral angle of 8.10°. The two oxygen atoms O(1) and O(3) are closer to the pyridyl ring bearing N(1), but the O(2) and O(4) are slightly away titled from the pyridyl ring bearing N(2), resulting in different extent of steric repulsion between the oxygen atom and the ppy as reflected in the significantly different Ir−N(1) and Ir−N(2) bond distances of 2.081(7) and 2.059(7) Å, respectively. The Ir−S bond distances are close to those reported for Ir(III)−S complexes.[30] The S−O distances (1.477(6), 1.467(6), 1.471(6), and 1.485(6) Å) and O═S═O angles (111.7(4)° and 112.1(4)°) are in the range observed for other sulfinates (1.431−1.490 Å; 111.7°−116.1°).[9a,c,18,31,32]

DFT Modeling. Different functionals and basis sets including B3LYP/(6-31G(d) + LANL2DZ), B3LYP/(6-31G(d) + SDD), B3PW91/(6-31G(d) + LANL2DZ), and B3PW91/(6-31G(d) + SDD) were used to calculate the electronic structures and to model the molecular structures of the iridium complexes. On the whole, they give similar results. As the method B3PW91/(6-31G(d) + SDD) gives the best agreement with the experimentally determined structure of $[\mathbf{IrSO_2SO_2}]^-$ and UV−vis absorption spectra of all three complexes, only its results are mentioned in the following discussion.

Selected bond lengths and angles of the optimized structures (Figure 6) of $[\mathbf{IrSS}]^-$, $[\mathbf{IrSSO_2}]^-$, and $[\mathbf{IrSO_2SO_2}]^-$ are listed in Table 3. The optimized structure of $[\mathbf{IrSS}]^-$ (Figure 6a) shows a C_2 symmetry as suggested by the ^1H NMR of the complex. The IrS_2C_2 ring is planar as in the case of Cp*Ir(benzene-1,2-dithiolate)[33a] and related d^6 Ru(II)[33b,c] and Os(II)[33d] complexes. The calculated Ir−S bond distance (2.457 Å) is similar to that in $[Ir(ppy)_2$(2-(benzylideneamino)-benzenethiolate)][34] (2.447(2) Å) but much longer than those

dx.doi.org/10.1021/ic501278n | Inorg. Chem. 2014, 53, 9739−9750

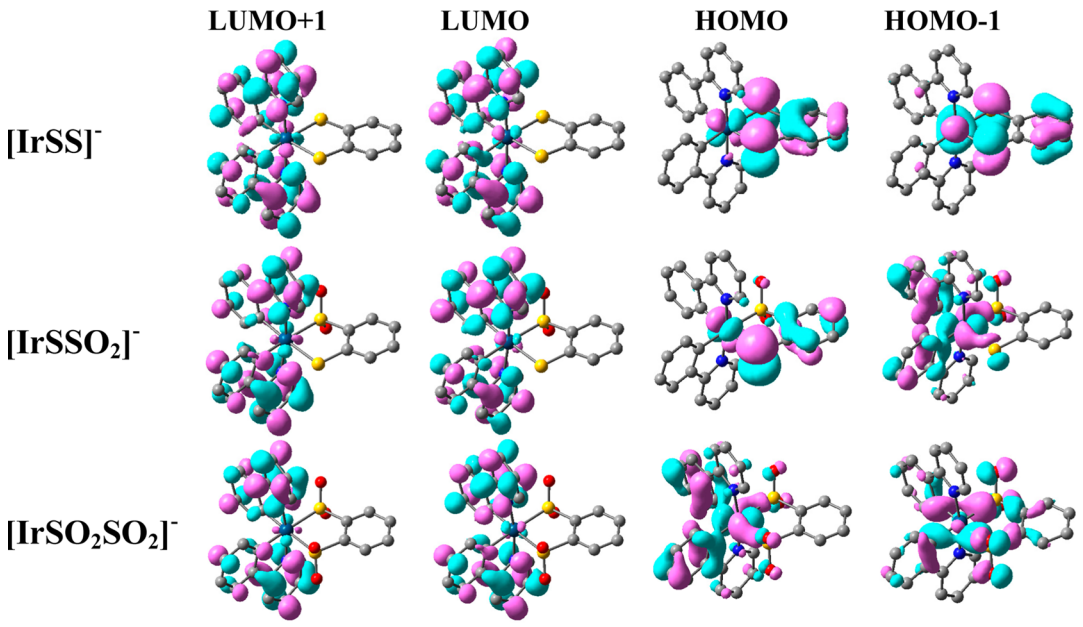

Figure 7. Frontier molecular orbital surfaces of $[IrSS]^-$, $[IrSSO_2]^-$, and $[IrSO_2SO_2]^-$ at the ground state optimized geometries. Surface isovalue is 0.035 au and hydrogen atoms are omitted for clarity.

Table 4. DFT-Calculated (B3PW91/(6-31G(d) + SDD)) One-Electron Energies and Compositions of HOMO−1, HOMO, LUMO, and LUMO+1 of $[IrSS]^-$, $[IrSSO_2]^-$, and $[IrSO_2SO_2]^-$

		MO composition (%)							
orbital	energy (eV)	Ir (s, p)	Ir (d)	ppy (*trans* to S)	ppy (*trans* to SO_2)	S	$S(SO_2)$	O	thiolate phenyl
				$[IrSS]^-$					
LUMO+1	−1.30	0.53	3.72	94.56	*a*	1.09	*a*	*a*	0.09
LUMO	−1.34	1.04	2.47	95.32	*a*	0.98	*a*	*a*	0.19
HOMO	−4.30	1.17	11.95	3.88	*a*	56.80	*a*	*a*	26.20
HOMO−1	−4.95	0.46	29.32	9.62	*a*	39.18	*a*	*a*	21.42
				$[IrSSO_2]^-$					
LUMO+1	−1.38	0.77	3.13	37.70	57.24	0.63	0.25	0.22	0.07
LUMO	−1.42	1.20	2.04	57.76	37.8	0.38	0.27	0.18	0.37
HOMO	−4.90	0.36	18.33	3.22	1.57	50.20	0.05	1.51	24.76
HOMO−1	−5.37	0.59	31.52	29.20	24.71	5.29	2.07	5.13	1.49
				$[IrSO_2SO_2]^-$					
LUMO+1	−1.49	1.28	2.39	*a*	95.32	*a*	0.43	0.50	0.09
LUMO	−1.49	1.28	1.74	*a*	95.80	*a*	0.48	0.29	0.41
HOMO	−5.59	0.29	27.60	*a*	60.56	*a*	3.50	7.59	0.45
HOMO−1	−5.78	4.10	1.14	*a*	36.51	*a*	11.80	36.39	10.06

[a]Not applicable.

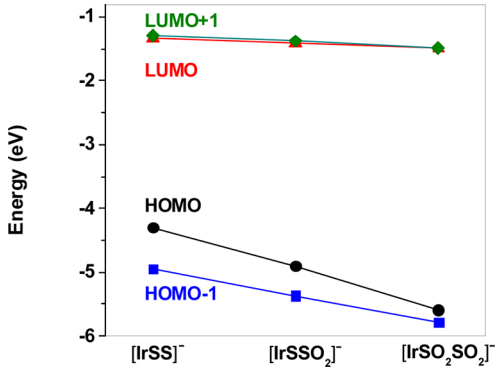

Figure 8. Plot of the energies of the frontier orbitals of the complexes.

in Cp*Ir(benzene-1,2-dithiolate)[33b] (2.235(4) Å) probably due to the strong *trans*-influence of the ppy ligand.

The optimized structure of $[IrSSO_2]^-$ (Figure 6b) shows no symmetry. Accordingly, the two sulfinate oxygen atoms are diastereoptic, having different chemical environment with one (O1) being close to the edge of a ppy ligand but the other (O2) is not. To minimize steric repulsion between the O atom and the peripheral H atoms of the ppy ring, the SO_2S-phenyl ring is canted, showing a dihedral angle of 8° with the IrS_2 plane. The optimized structure of $[IrSO_2SO_2]^-$ (Figure 6c) resembles closely the crystal structure, showing similar bond lengths, bond angles, and a C_2 symmetry. The calculated S═O (∼1.5 Å) and Ir−S(O_2) (2.405 Å) distances in the two sulfinate complexes are close to those observed in the crystal structure of $[IrSO_2SO_2]^-$ (1.467(6) −1.485(6) Å and 2.348(2) Å).

dx.doi.org/10.1021/ic501278n | *Inorg. Chem.* 2014, 53, 9739−9750

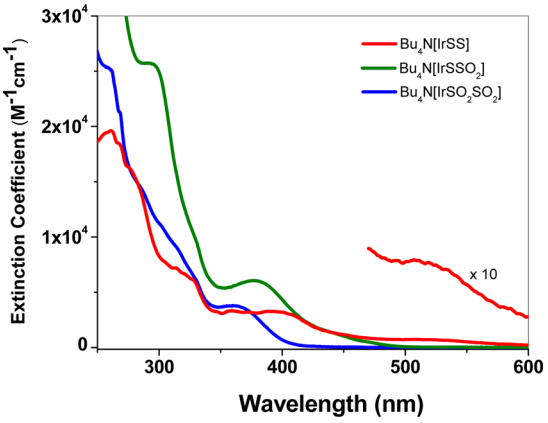

Figure 9. UV–vis absorption spectra of ^{n}Bu$_4$N[**IrSS**] (red), ^{n}Bu$_4$N-[**IrSSO$_2$**] (green), and ^{n}Bu$_4$N[**IrSO$_2$SO$_2$**] (blue) in CH$_3$CN at room temperature.

While all the three structures show similar Ir–N bond lengths, the calculated Ir–C bond lengths are different significantly with the Ir–C bond *trans* to thiolate showing shorter distance (2.032 Å) than the Ir–C bond *trans* to sulfinate (bond length of 2.043 and 2.045 Å). Our DFT calculation gives Mayer bond orders of the Ir–C bonds *trans* to thiolate S in [**IrSS**]$^-$ and [**IrSSO$_2$**]$^-$ as 0.77 and 0.74, but for the Ir–C bonds *trans* to sulfinate S in [**IrSSO$_2$**]$^-$ and [**IrSO$_2$SO$_2$**]$^-$, our calculation gives lower bond orders of 0.70 and 0.71. It can be explained by the decrease of Ir-to-ppy π-back bonding as the strongly electron-donating thiolate is converted to weakly donating sulfinate. Grapperhaus et al.[9c] made a similar observation that the Ru–P bond in the complex (4,7-bis(2′-methyl-2′-mercaptopropyl)-1-thia-4,7-diazacyclononane)RuPPh$_3$, is elongated as the sulfur atoms are oxygenated to sulfenate S=O and sulfinate SO$_2$, and the reason is that the antibonding filled dπ(Ru)–pπ(S) interactions, which enhance Ru-to-P π-back bonding, are removed by the oxidations.

For d^6 or d^8 metal–thiolate and sulfinate complexes, the fact that the metal–S(thiolate) bond is invariably longer than the corresponding metal–S(sulfinate) bond is accounted by the removal of the repulsive filled dπ–pπ interactions by dioxygenation,[9a,17c,35] and decrease in the atomic radius from S(0) in thiolate to S(IV) in sulfinate. Our DFT calculations also give Ir–S(thiolate) distances (2.457 Å for [**IrSS**]$^-$ and 2.468 Å for [**IrSSO$_2$**]$^-$) that are longer than the Ir–S(sulfinate) bonds in the oxygenated complexes (calculated = 2.405 Å, experimental = 2.348(2) Å). In accord with the notion that thiolate is a stronger σ-donor than sulfinate,[9a] the calculated Mayer bond order for Ir–S(thiolate) bonds in [**IrSS**]$^-$ and [**IrSSO$_2$**]$^-$ (0.76 and 0.74) is markedly higher than that of Ir–S(O$_2$) bonds in [**IrSSO$_2$**]$^-$ and [**IrSO$_2$SO$_2$**]$^-$ (0.65 and 0.66).

Electronic Structures. The HOMO, HOMO−1, LUMO, and LUMO+1 of the complexes are shown in Figure 7 and their compositions are listed in Table 4. For all three complexes, the LUMO, LUMO+1, LUMO+2, and LUMO+3 are predominantly π^* orbitals of ppy. The LUMO and LUMO +1 are close in energy E (ΔE = 0.04 eV for [**IrSS**]$^-$ and [**IrSSO$_2$**]$^-$ and ∼0 eV for [**IrSO$_2$SO$_2$**]$^-$) and are lower in energy than the LUMO+2 and LUMO+3 by >0.8 eV. Like d^8- and other d^6-thiolates with completely filled t$_{2g}$ orbitals, the HOMO of [**IrSS**]$^-$ is an antibonding combination of the 5d$_{xz}$ orbital and the 3p$_x$ orbitals (lone pairs) of the two S atoms of the benzenedithiolate which are involved in antibonding interactions with a π orbital of the conjugated phenyl ring (the z-axis is designated to the C_2 axis and the x-axis is perpendicular to the S$_2$-phenyl ring). The HOMO is mainly composed of the 3p$_x$ orbitals of the S atoms with small contribution from the phenyl ring orbital and even smaller contribution from 5d$_{xz}$ orbital. The HOMO−1 is also dominated by the lone pairs of the S atoms but with more contribution from the dπ orbital of Ir than the HOMO. The HOMO−2 mainly consists of the metal d-orbital and π-bonding orbital of ppy. The HOMO and HOMO−1 are separated by 0.65 eV.

Similar to [**IrSS**]$^-$, the HOMO of [**IrSSO$_2$**]$^-$ mainly consists of the lone pair of the thiolate S atom, which is involved in antibonding interactions with the 5d$_{xz}$ orbital of Ir and a π^*-orbital of the phenyl ring. Unlike [**IrSS**]$^-$, the HOMO−1 of [**IrSSO$_2$**]$^-$ is mainly composed of a π-orbital of ppy and a metal d orbital, and the contribution from the S lone pair is negligibly small. It is significantly lower in energy than the HOMO by 0.5 eV.

The HOMO of [**IrSO$_2$SO$_2$**]$^-$ resembles that of heteroleptic Ir(ppy)$_2$L where L is primarily σ-donor,[1c,3b,36] being largely composed of a π-orbital of ppy with significant contribution from a metal d-orbital. On the other hand, the HOMO−1 has significant contribution from the bonding orbitals of the two S=O bonds and the π-orbitals of ppy. The HOMO and HOMO−1 are different by 0.2 eV.

Table 5. Absorption and Emission Data of the Complexes

	absorption maxima				
compound	nm (ε/10^3 M^{-1}cm^{-1})	eV	emission maxima/nm (eV)	emission lifetime, τ/ns	emission quantum yield, Φ
^{n}Bu$_4$N[**IrSS**]	510 (0.5)	2.43	665 (1.86)	20	∼ 0.005
	400 (3.0)	3.10			
	328 (5.8)	3.78			
	315 (6.8)	3.94			
	277 (15.8)	4.48			
^{n}Bu$_4$N[**IrSSO$_2$**]	440 (1.4)	2.82	556 (2.23)	120	0.13
	380 (6.0)	3.26			
	330 (9.6)	3.76			
	294 (25.7)	4.22			
^{n}Bu$_4$N[**IrSO$_2$SO$_2$**]	362 (3.8)	3.43	460 (2.70)	890	0.62
	329 (6.3)	3.77			
	260 (25.2)	4.77			

dx.doi.org/10.1021/ic501278n | Inorg. Chem. 2014, 53, 9739–9750

Table 6. TD-DFT (B3PW91/(6-31G(d) + SDD)) Calculated Singlet Excitation Energies (eV) for $[IrSS]^-$, $[IrSSO_2]^-$, and $[IrSO_2SO_2]^-$ in CH_3CN

complex	excitation energy/nm (eV)	oscillator strength	transition[a]	contribution (%)
$[IrSS]^-$	535 (2.32)	0.0026	HOMO→LUMO	100
	527 (2.35)	0.0087	HOMO→LUMO+1	100
	436 (2.84)	0.0027	HOMO→LUMO+2	98
	430 (2.88)	0.0102	HOMO−1→LUMO	90
	404 (3.07)	0.0800	HOMO−2→LUMO	88
	394 (3.15)	0.0023	HOMO−2→LUMO+1	94
	357 (3.47)	0.0185	HOMO−1→LUMO+2	93
$[IrSSO_2]^-$	442 (2.81)	0.0027	HOMO→LUMO	92
	437 (2.84)	0.0056	HOMO→LUMO+1	92
	391 (3.17)	0.0635	HOMO−1→LUMO	96
	383 (3.24)	0.0113	HOMO−1→LUMO+1	94
	369 (3.36)	0.0110	HOMO→LUMO+2	96
	355 (3.49)	0.0047	HOMO→LUMO+3	95
$[IrSO_2SO_2]^-$	376 (3.30)	0.0730	HOMO→LUMO	98
	345 (3.59)	0.0244	HOMO−1→LUMO+1	99
	344 (3.60)	0.0097	HOMO−1→LUMO	99
	320 (3.87)	0.0148	HOMO→LUMO+2	97
	312 (3.97)	0.0260	HOMO−3→LUMO+1	59
			HOMO→LUMO+3	30
	311 (3.99)	0.0139	HOMO−3→LUMO	88

[a]Only major transitions are shown.

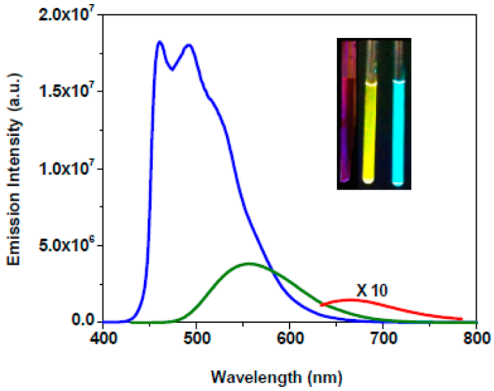

Figure 10. Emission spectra of degassed CH_3CN solutions of $^nBu_4N[IrSS]$ (red), $^nBu_4N[IrSSO_2]$ (green), and $^nBu_4N[IrSO_2SO_2]$ (blue) at room temperature (excitation wavelength = 420, 420, and 370 nm, respectively). (inset) From left to right, the emission colors of $^nBu_4N[IrSS]$, $^nBu_4N[IrSSO_2]$, and $^nBu_4N[IrSO_2SO_2]$.

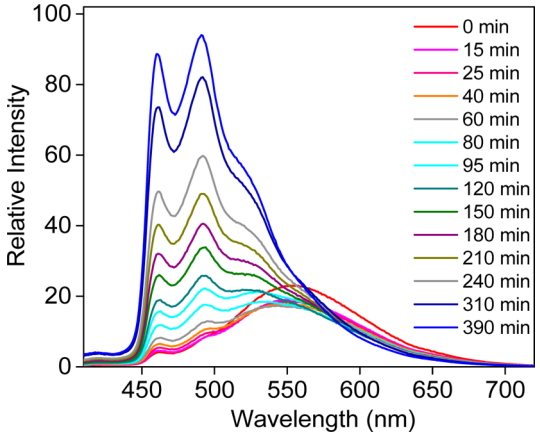

Figure 11. Overlaid emission spectra recorded at different times after exposing a degassed CH_3CN solution of $^nBu_4N[IrSSO_2]$ to air.

Examining the energy of the frontier orbitals of the three complexes (Figure 8) shows that the energies of the LUMO and LUMO+1 are not much affected by the S → SO_2 oxidation as they only drop by ∼0.08 eV per dioxygenation. As the orbitals are largely localized in ppy, the dioxygenation can only have an indirect effect on their energies, primarily through an increase in electrostatic attraction of Ir ion. On the other hand, the energies of the HOMO and HOMO−1 are sensitive to the oxidation with each dioxygenation brings about ∼0.6 eV and ∼0.4 eV drop to the energies of the orbitals, respectively. The decrease of the HOMO energy from $[IrSS]^-$ to $[IrSSO_2]^-$ is due to an increase in Coulombic interaction as sulfinate is a weaker electron donor than thiolate and a decrease in orbital (antibonding dπ−pπ) interactions between the lone pair of the S atom in $[IrSSO_2]^-$ and the metal dπ orbital as the energy gap between them is widened. The HOMO of $[IrSO_2SO_2]^-$ is mainly composed of metal d-orbital, which is more stabilized than the S lone pairs in the other two complexes. Consequently, there is a widening of the HOMO−LUMO gap as the S atoms are dioxygenated, which is translated into blue shift in UV−vis absorption and emission of the complexes, as will be discussed in the next section.

UV−vis Absorption. Figure 9 shows the UV−vis absorption spectra of the three complexes in CH_3CN at room temperature, and Table 5 summarizes the spectral and photophysical data. Energies, orbital percentages, and oscillator strength of major spin-allowed electronic transitions in CH_3CN obtained from TD-DFT calculations are listed in Table 6.

All three spectra display intense absorptions in near-UV region (<350 nm, $\varepsilon \approx 10^3$−10^4 M^{-1} cm^{-1}) that are due to intraligand $\pi \rightarrow \pi^*$ transitions and higher energy metal-to-ligand(π^* of ppy)-charge-transfer (MLCT) transition. The spectrum of $[IrSS]^-$ shows a broad, weak absorption at 510 nm (ε_{max} = 520 $M^{-1}cm^{-1}$) which comprise the HOMO → LUMO and HOMO → LUMO+1 transitions. Given the nature of the orbitals, the transitions can be described as ligand (3p of S)-to-

dx.doi.org/10.1021/ic501278n | Inorg. Chem. 2014, 53, 9739−9750

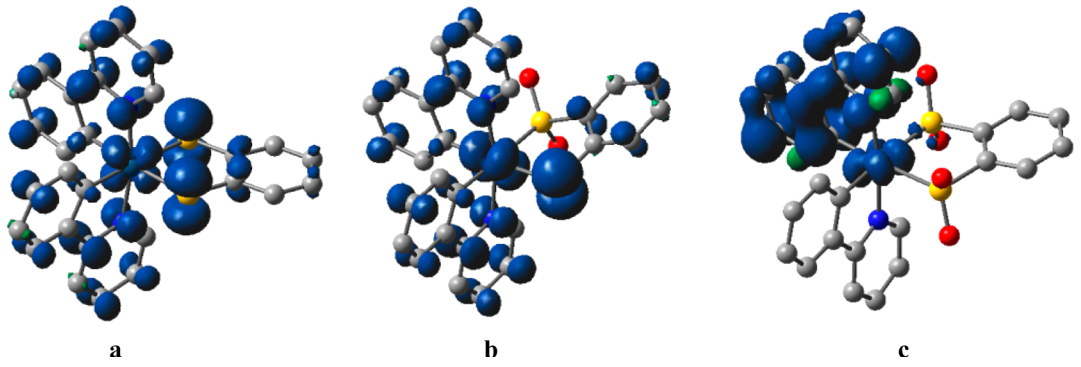

Figure 12. Surface plots of the spin-density distribution of the optimized T_1 states of $[\mathbf{IrSS}]^-$, $[\mathbf{IrSSO_2}]^-$, and $[\mathbf{IrSO_2SO_2}]^-$ using DFT at UB3PW91/(6-31G(d)+SDD) level. Surface isovalue is 0.005 au and hydrogen atoms are omitted.

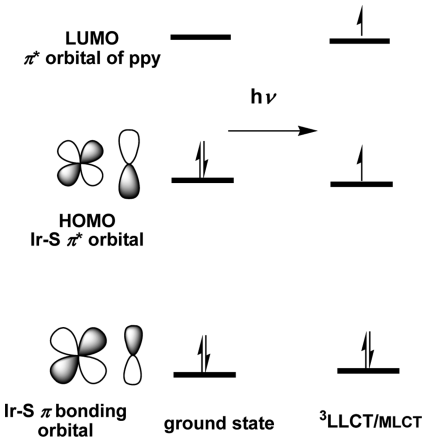

Figure 13. Molecular orbital diagram showing formation of partial Ir–S π bond in the ^{3}LLCT/MLCT excited state of $[\mathbf{IrSSO_2}]^-$.

ligand(π^* of ppy)-charge-transfer (LLCT) with a *small* MLCT character and is labeled LLCT/MLCT in this study. The low extinction coefficient of the transitions is due to poor overlap between the mostly thiolate-based donor orbitals and mostly ppy-based acceptor orbitals involved.[37] A similar case would be *fac*-[Re(NHPh)(CO)$_3$(bipy)] reported by Záliš and Vlček which exhibits a low energy, weak LLCT absorption (NPhH → π^* of bipy; λ_{max} = 620 nm, ε_{max} = 280 M^{-1} cm^{-1}).[38] A moderately intense absorption band ranges from ~450 nm to ~380 nm (λ_{max} = 400 nm, ε_{max} = 3.0 × 10^3 M^{-1} cm^{-1}). The absorption is derived from a two LLCT/MLCT transitions (HOMO → LUMO+2, calculated λ_{max} = 436 nm; HOMO−1 → LUMO, calculated λ_{max} = 430 nm) and two MLCT/$\pi\pi^*$ transitions (HOMO−2 → LUMO, calculated λ_{max} = 404 nm; HOMO−2 → LUMO+1, calculated λ_{max} = 394 nm).

The absorption spectrum of $[\mathbf{IrSSO_2}]^-$ displays a tailing around 440 nm ($\varepsilon \approx 1.4 \times 10^3$ M^{-1} cm^{-1}) arising from LLCT/MLCT transitions (HOMO → LUMO, HOMO → LUMO +1). The transitions are blue-shifted from those of $[\mathbf{IrSS}]^-$ by ~3000 cm^{-1} (0.37 eV). An intense absorption at 380 nm (ε_{max} = 6.0 × 10^3 M^{-1} cm^{-1}) is derived from the HOMO−1 → LUMO, LUMO+1 transitions which are MLCT/$\pi\pi^*$ in nature.

The spectrum of $[\mathbf{IrSO_2SO_2}]^-$ resembles that of *fac*-$[Ir(ppy)_3]$[1b,39] (λ_{max} = 377 nm) and the heteroleptic $[Ir(ppy)_2(bipy)]PF_6$[40] (λ_{max} = 375 nm) showing an intense band at 362 nm (ε_{max} = 3.77 × 10^3 M^{-1} cm^{-1}) which is the MLCT/$\pi\pi^*$ HOMO → LUMO transition. The intense absorptions at <320 nm are due to high-energy MLCT/$\pi\pi^*$ transitions.

The calculated spectra (Supporting Information, Figure S7) reproduce the salient features of the experimental ones, especially the low-energy LLCT/MLCT bands and the MLCT/$\pi\pi^*$ bands.

Emission. All three complexes display emissions in degassed CH_3CN solutions, and their emission energy and intensity follow the order of $[\mathbf{IrSO_2SO_2}]^-$ > $[\mathbf{IrSSO_2}]^-$ ≫ $[\mathbf{IrSS}]^-$ (Figure 10 and Table 5). Exposing a degassed solution of ^{n}Bu$_4$N[**IrSS**] to air leads to immediate disappearance of the 665 nm emission, which is accompanied by appearance of $[\mathbf{IrSSO_2}]^-$ emission and, in smaller part, $[\mathbf{IrSO_2SO_2}]^-$ emission. The intensity of $[\mathbf{IrSO_2SO_2}]^-$ emission slowly increases at the expense of $[\mathbf{IrSSO_2}]^-$ emission (Figure 11).

Unrestricted Kohn–Sham calculations were performed to obtain optimized structures of the lowest-energy triplet excited states (T_1) of the complexes. Selected structural parameters and the energies of T_1 obtained from ΔSCF calculations and TD-DFT formalism are listed in Table S1 (Supporting Information). Surface plots of the spin-density distribution of the optimized T_1 states are shown in Figure 12.

Solution of $[\mathbf{IrSO_2SO_2}]^-$ shows an intense vibronic luminescence at 460 nm with long emission lifetime of 0.89 μs, which suggests possible triplet nature of the emissive excited state. In fact, the vibronic feature and energy of the emission are similar to the ^{3}MLCT/$\pi\pi^*$ emissions of *fac*-$[Ir(ppy)_3]$ and related complexes.[2b,41] The optimized T_1 state of the complex, which arises from the HOMO → LUMO (68%) and HOMO−2 → LUMO excitations, shows a distortion from the ground state C_2 symmetry. The T_1 state shows spin density on the ppy ligand and the metal ion (Figure 12c), which is consistent with an MLCT/$\pi\pi^*$ assigment. The $T_1 \rightarrow S_0$ (singlet ground state) emission energy calculated using ΔSCF method (505 nm, 2.46 eV) is close to the observed emission peak (492 nm, 2.52 eV), while the TD-DFT calculation gives a lower energy (543 nm, 2.28 eV). Solution of $[\mathbf{IrSS}]^-$ shows a very weak, broad red emission peaked at 665 nm. The yellow emission of $[\mathbf{IrSSO_2}]^-$ shows no vibronic feature and occurs at lower energy (λ_{max} = 556 nm) with a lower quantum yield, suggesting that it is derived from an excited state other than ^{3}MLCT/$\pi\pi^*$. The fact that in the presence of air, the emissions of the complexes undergo changes (Figure 11) that are in parallel with the dioxygenation chemistry of the complexes supports the notion that the lone pairs of the S atoms are involved in the generation of the emissive excited states of $[\mathbf{IrSS}]^-$ and $[\mathbf{IrSSO_2}]^-$. The calculated T_1 states of the complexes arise almost entirely from the HOMO → LUMO transitions, show spin densities at the thiolate sulfur atoms, the ppy ligands, and the Ir ion, indicating

dx.doi.org/10.1021/ic501278n | Inorg. Chem. 2014, 53, 9739–9750

their ^{3}LLCT/MLCT character. The calculated energies of the $T_1 \rightarrow S_0$ transitions of the complexes (for $[\mathbf{IrSS}]^-$, ΔSCF: 657 nm or 1.89 eV and TD-DFT: 671 nm or 1.85 eV; for $[\mathbf{IrSSO_2}]^-$, ΔSCF: 527 nm or 2.35 eV; TD-DFT: 543 nm or 2.28 eV) are close to their emission maxima (for $[\mathbf{IrSS}]^-$, λ_{max} = 665 nm or 1.86 eV; for $[\mathbf{IrSSO_2}]^-$, λ_{max} = 543 nm or 2.28 eV).

The Ir−S(thiolate) bonds in the T_1 states of $[\mathbf{IrSSO_2}]^-$ and $[\mathbf{IrSS}]^-$ are significantly shorter than the corresponding ones in their singlet ground states S_0, indicating an increase in Ir−S(thiolate) bond order in the excited states. It is consistent with the fact that the excited states arise from HOMO → LUMO excitations, which involve promotion of an electron in the antibonding π^* orbital of the Ir−S bond (HOMO) to a π^* orbital of ppy (LUMO) (see Figure 13). Depopulation of electron density in the Ir−S π^* orbital would lead to a partial π bond in addition to the existing Ir−S σ bond and thus an increase in formal bond order.

CONCLUSION

We demonstrated in this study the high reactivity of the anionic $[\mathbf{IrSS}]^-$ complex toward dioxygenation, which is due to the destabilization of the HOMO, which is mainly composed of the lone pairs of the S atoms, by the so-called filled dπ−pπ antibonding interactions. The first dioxygenation product sulfinate−thiolate complex $[\mathbf{IrSSO_2}]^-$ can be further oxidized to disulfinate complex $[\mathbf{IrSO_2SO_2}]^-$. The reaction leads to stabilization of the HOMOs of the complexes and a change in the nature of the orbitals from thiolate-centered in $[\mathbf{IrSS}]^-$ and $[\mathbf{IrSSO_2}]^-$ to metal/ppy-centered in $[\mathbf{IrSO_2SO_2}]^-$. These changes lead to drastically different emission colors and other photophysical properties. However, the complex $[\mathbf{IrSS}]^-$ cannot be used as sensor for ROS as it is simply too reactive toward oxygen. Nonetheless, the fact that $[\mathbf{IrSS}]^-$ is highly susceptible to oxidation suggests the two S atoms could be very nucleophilic. It is therefore probable that the complex can undergo alkylation readily and can act as "metalloligand" by donating the lone pairs of the S atoms to metal ions and Lewis acids in forming multimetallic luminescent supramolecules. Work along this direction is now being pursued in our laboratory.

ASSOCIATED CONTENT

Supporting Information

2D-COSY spectra and ESI-MS of the complexes, TD-DFT calculated absorption spectra, and selected structural parameters of the lowest-energy triplet excited states are available free of charge via the Internet at http://pubs.acs.org.

AUTHOR INFORMATION

Corresponding Author

*E-mail: chmyiphk@nus.edu.sg.

Notes

The authors declare no competing financial interest.

ACKNOWLEDGMENTS

We are grateful to Prof. L. L. Koh and Ms. T. G. Kheng for determining the X-ray structures. The Ministry of Education (R-143-000-548-112) Singapore and the National University of Singapore are thanked for financial support.

REFERENCES

(1) (a) Sprouse, S.; King, K. A.; Spellane, P. J.; Watts, R. J. *J. Am. Chem. Soc.* **1984**, *106*, 6647. (b) Tamayo, A. B.; Alleyne, B. D.; Djurovich, P. I.; Lamansky, S.; Tsyba, I.; Ho, N. N.; Bau, R.; Thompson, M. E. *J. Am. Chem. Soc.* **2003**, *125*, 7377. (c) Li, J.; Djurovich, P. I.; Alleyne, B. D.; Yousufuddin, M.; Ho, N. N.; Thomas, J. C.; Peters, J. C.; Bau, R.; Thompson, M. E. *Inorg. Chem.* **2005**, *44*, 1713. (d) Coppo, P.; Plummer, R. A.; De Cola, L. *Chem. Commun.* **2004**, 1774. (e) Coppo, P.; Duati, M.; Kozhevnikov, V. N.; Hofstraat, J. W.; De Cola, L. *Angew. Chem., Int. Ed.* **2005**, *44*, 1806. (f) Ladouceur, S.; Zysman-Colman, E. *Eur. J. Inorg. Chem.* **2013**, 2985. (g) You, Y.; Nam, W. *Chem. Soc. Rev.* **2012**, *41*, 7061.

(2) (a) Baldo, M. A.; Thompson, M. E.; Forrest, S. R. *Nature* **2000**, *403*, 750. (b) Lowry, M. S.; Bernhard, S. *Chem.—Eur. J.* **2006**, *12*, 7970. (c) Tsuboyama, A.; Okada, S.; Ueno, K. *Highly Efficient OLEDs with Phosphorescent Materials;* Wiley-VCH: Weinheim, Germany, 2008. (d) Lamansky, S.; Djurovich, P.; Murphy, D.; Abdel-Razzaq, F.; Lee, H.-E.; Adachi, C.; Burrows, P. E.; Forrest, S. R.; Thompson, M. E. *J. Am. Chem. Soc.* **2001**, *123*, 4304. (e) Lamansky, S.; Djurovich, P.; Murphy, D.; Abdel-Razzaq, F.; Kwong, R.; Tsyba, I.; Bortz, M.; Mui, B.; Bau, R.; Thompson, M. E. *Inorg. Chem.* **2001**, *40*, 1704. (f) Nazeeruddin, M. K.; Humphry-Baker, R.; Berner, D.; Rivier, S.; Zuppiroli, L.; Grätzel, M. *J. Am. Chem. Soc.* **2003**, *125*, 8790. (g) D'Andrade, B. W.; Holmes, R. J.; Forrest, S. R. *Adv. Mater.* **2004**, *16*, 624. (h) Grushin, V. V.; Herron, N.; LeCloux, D. D.; Marshall, W. J.; Petrov, V. A.; Wang, Y. *Chem. Commun.* **2001**, 1494. (i) Karatsu, T.; Takahashi, M.; Yagai, S.; Kitamura, A. *Inorg. Chem.* **2013**, *52*, 12338. (j) Chen, H.-F.; Wu, C.; Kuo, M.-C.; Thompson, M. E.; Wong, K.-T. *J. Mater. Chem.* **2012**, *22*, 9556.

(3) (a) Goldsmith, J. I.; Hudson, W. R.; Lowry, M. S.; Anderson, T. H.; Bernhard, S. *J. Am. Chem. Soc.* **2005**, *127*, 7502. (b) Tinker, L. L.; Bernhard, S. *Inorg. Chem.* **2009**, *48*, 10507. (c) Yuan, Y.-J.; Zhang, J.-Y.; Yu, Z.-T.; Feng, J.-Y.; Luo, W.-J.; Ye, J.-H.; Zou, Z.-G. *Inorg. Chem.* **2012**, *51*, 4123. (d) Nagib, D. A.; Scott, M. E.; MacMillan, D. W. C. *J. Am. Chem. Soc.* **2009**, *131*, 10875. (e) Sato, S.; Morikawa, T.; Kajino, T.; Ishitani, O. *Angew. Chem., Int. Ed.* **2013**, *52*, 988. (f) Whang, D. R.; Sakai, K.; Park, S. Y. *Angew. Chem., Int. Ed.* **2013**, *52*, 11612.

(4) (a) Mayo, E. I.; Kilsa, K.; Tirrell, T.; Djurovich, P. I.; Tamayo, A.; Thompson, M. E.; Lewis, N. S.; Gray, H. B. *Photochem. Photobiol. Sci.* **2006**, *5*, 871. (b) Baranoff, E.; Yum, J.-H.; Jung, I.; Vulcano, R.; Grätzel, M.; Nazeeruddin, M. K. *Chem.—Asian J.* **2010**, *5*, 496.

(5) (a) Schulz, G. L.; Holdcroft, S. *Chem. Mater.* **2008**, *20*, 5351. (b) Fleetham, T. B.; Wang, Z.; Li, J. *Inorg. Chem.* **2013**, *52*, 7338. (c) Baranoff, E.; Yum, J.-H.; Graetzel, M.; Nazeeruddin, M. K. *J. Organomet. Chem.* **2009**, *694*, 2661.

(6) (a) You, Y.; Han, Y.; Lee, Y.-M.; Park, S. Y.; Nam, W.; Lippard, S. J. *J. Am. Chem. Soc.* **2011**, *133*, 11488. (b) Lee, P.-K.; Law, W. H.-T.; Liu, H.-W.; Lo, K. K.-W. *Inorg. Chem.* **2011**, *50*, 8570. (c) Lo, K. K.-W.; Chung, C.-K.; Lee, T. K.-M.; Lui, L.-H.; Tsang, K. H.-K.; Zhu, N. *Inorg. Chem.* **2003**, *42*, 6886. (d) Li, C.; Yu, M.; Sun, Y.; Wu, Y.; Huang, C.; Li, F. *J. Am. Chem. Soc.* **2011**, *133*, 11231. (e) Woo, H.; Cho, S.; Han, Y.; Chae, W.-S.; Ahn, D.-R.; You, Y.; Nam, W. *J. Am. Chem. Soc.* **2013**, *135*, 4771. (f) Moromizato, S.; Hisamatsu, Y.; Suzuki, T.; Matsuo, Y.; Abe, R.; Aoki, S. *Inorg. Chem.* **2012**, *51*, 12697.

(7) (a) Mak, C. S. K.; Hayer, A.; Pascu, S. I.; Watkins, S. E.; Holmes, A. B.; Kohler, A.; Friend, R. H. *Chem. Commun.* **2005**, 4708. (b) Ladouceur, S.; Fortin, D.; Zysman-Colman, E. *Inorg. Chem.* **2011**, *50*, 11514. (c) Tsuchiya, K.; Yagai, S.; Kitamura, A.; Karatsu, T.; Endo, K.; Mizukami, J.; Akiyama, S.; Yabe, M. *Eur. J. Inorg. Chem.* **2010**, 926. (d) Stagni, S.; Colella, S.; Palazzi, A.; Valenti, G.; Zacchini, S.; Paolucci, F.; Marcaccio, M.; Albuquerque, R. Q.; De Cola, L. *Inorg. Chem.* **2008**, *47*, 10509.

(8) (a) Stiefel, E. I. *Pure Appl. Chem.* **1998**, *70*, 889. (b) Bethel, R. D.; Darensbourg, M. Y. *Nature* **2013**, *499*, 40.

(9) (a) Buonomo, R. M.; Font, I.; Maguire, M. J.; Reibenspies, J. H.; Tuntulani, T.; Darensbourg, M. Y. *J. Am. Chem. Soc.* **1995**, *117*, 963. (b) Masitas, C. S. A.; Mashuta, M. S.; Grapperhaus, C. A. *Inorg. Chem.* **2010**, *49*, 5344. (c) Masitas, C. S. A.; Kumar, M.; Mashuta, M. S.; Kozlowski, P. M.; Grapperhaus, C. A. *Inorg. Chem.* **2010**, *49*, 10875.

(d) Grapperhaus, C. A.; Darensbourg, M. Y. *Acc. Chem. Res.* **1998**, *31*, 451. (e) Herdt, D. R.; Grapperhaus, C. A. *Dalton Trans.* **2012**, *41*, 364. (f) Shin, R. Y. C.; Goh, L. Y. *Acc. Chem. Res.* **2006**, *39*, 301. (g) Connick, W. B.; Gray, H. B. *J. Am. Chem. Soc.* **1997**, *119*, 11620.
(10) (a) King, R. B.; Bisnette, M. B. *Inorg. Chem.* **1965**, *4*, 482. (b) Ashby, M. T.; Enemark, J. H.; Lichtenberger, D. L. *Inorg. Chem.* **1988**, *27*, 191. (c) Gennari, M.; Orio, M.; Pécaut, J.; Bothe, E.; Neese, F.; Collomb, M.-N. L.; Duboc, C. *Inorg. Chem.* **2011**, *50*, 3707. (d) Fox, D. C.; Fiedler, A. T.; Halfen, H. L.; Brunold, T. C.; Halfen, J. A. *J. Am. Chem. Soc.* **2004**, *126*, 7627. (e) Shin, R. Y. C.; Teo, M. E.; Leong, W. K.; Vittal, J. J.; Yip, J. H. K.; Goh, L. Y.; Webster, R. D. *Organometallics* **2005**, *24*, 1483.
(11) (a) Lee, T. K.-M.; Zhu, N.; Yam, V. W.-W. *J. Am. Chem. Soc.* **2010**, *132*, 17646. (b) Suardi, G.; Cleary, B. P.; Duckett, S. B.; Sleigh, C.; Rau, M.; Reed, E. W.; Lohman, J. A. B.; Eisenberg, R. *J. Am. Chem. Soc.* **1997**, *119*, 7716. (c) Xu, H.; Yip, J. H. K. *Inorg. Chem.* **2003**, *42*, 4492. (d) Forward, J. M.; Bohmann, D.; Fackler, J. P.; Staples, R. J. *Inorg. Chem.* **1995**, *34*, 6330. (e) Langer, R.; Yadav, M.; Weinert, B.; Fenske, D.; Fuhr, O. *Eur. J. Inorg. Chem.* **2013**, *2013*, 3623.
(12) (a) Eisenberg, R.; Gray, H. B. *Inorg. Chem.* **2011**, *50*, 9741. (b) Sproules, S.; Wieghardt, K. *Coord. Chem. Rev.* **2011**, *255*, 837. (c) Wiebelhaus, N. J.; Cranswick, M. A.; Klein, E. L.; Lockett, L. T.; Lichtenberger, D. L.; Enemark, J. H. *Inorg. Chem.* **2011**, *50*, 11021.
(13) Sie, W.-S.; Jian, J.-Y.; Shiu, K.-B. *J. Chin. Chem. Soc.* **2011**, *58*, 611.
(14) Lau, M.-K.; Cheung, K.-M.; Zhang, Q.-F.; Song, Y.; Wong, W.-T.; Williams, I. D.; Leung, W.-H. *J. Organomet. Chem.* **2004**, *689*, 2401.
(15) Sie, W.-S.; Jian, J.-Y.; Su, T.-C.; Lee, G.-H.; Lee, H. M.; Shiu, K.-B. *J. Organomet. Chem.* **2008**, *693*, 1510.
(16) (a) Grapperhaus, C. A.; Darensbourg, M. Y.; Sumner, L. W.; Russell, D. H. *J. Am. Chem. Soc.* **1996**, *118*, 1791. (b) Darensbourg, M. Y.; Tuntulani, T.; Reibenspies, J. H. *Inorg. Chem.* **1995**, *34*, 6287. (c) Tuntulani, T.; Musie, G.; Reibenspies, J. H.; Darensbourg, M. Y. *Inorg. Chem.* **1995**, *34*, 6279.
(17) (a) Dey, A.; Chow, M.; Taniguchi, K.; Lugo-Mas, P.; Davin, S.; Maeda, M.; Kovacs, J. A.; Odaka, M.; Hodgson, K. O.; Hedman, B.; Solomon, E. I. *J. Am. Chem. Soc.* **2005**, *128*, 533. (b) Shearer, J.; Callan, P. E.; Masitas, C. A.; Grapperhaus, C. A. *Inorg. Chem.* **2012**, *51*, 6032. (c) Lugo-Mas, P.; Dey, A.; Xu, L.; Davin, S. D.; Benedict, J.; Kaminsky, W.; Hodgson, K. O.; Hedman, B.; Solomon, E. I.; Kovacs, J. A. *J. Am. Chem. Soc.* **2006**, *128*, 11211.
(18) Begum, R. A.; Farah, A. A.; Hunter, H. N.; Lever, A. B. P. *Inorg. Chem.* **2009**, *48*, 2018.
(19) (a) Claus Jacob, P. G. W. *Redox Signaling and Regulation in Biology and Medicine;* Wiley-VCH: Weinheim, Germany, 2009. (b) Paulsen, C. E.; Carroll, K. S. *Chem. Rev.* **2013**, *113*, 4633. (c) Veal, E. A.; Day, A. M.; Morgan, B. A. *Mol. Cell* **2007**, *26*, 1.
(20) Armarego, W. L. F.; Chai, C.; Armarego, W. L. F.; Chai, C. *Purification of Laboratory Chemicals,* 5th ed.; Elsevier: Amsterdam, 2003.
(21) (a) Bruker. *SMART&SAINT Software Reference Manuals;* Bruker AXS, Inc.: Madison, WI, USA, 2007. (b) Bruker. *SADABS: Software for Empirical Absorption Correction;* Bruker AXS, Inc.: Madison, WI, USA, 2001. (c) *SHELXTL Reference Manual, version 5.03;* Siemens Energy and Automation, Inc., Analytical Instrumentation: Madison, WI, 1996.
(22) Sheldrick, G. *Acta Crystallogr., Sect. A* **2008**, *64*, 112.
(23) (a) Becke, A. D. *J. Chem. Phys.* **1993**, *98*, 5648. (b) Perdew, J. P.; Wang, Y. *Phys. Rev. B* **1992**, *45*, 13244.
(24) Andrae, D.; Häußermann, U.; Dolg, M.; Stoll, H.; Preuß, H. *Theor. Chim. Acta* **1990**, *77*, 123.
(25) (a) Miertuš, S.; Scrocco, E.; Tomasi, J. *Chem. Phys.* **1981**, *55*, 117. (b) Pascual-ahuir, J. L.; Silla, E.; Tuñon, I. *J. Comput. Chem.* **1994**, *15*, 1127.
(26) Frisch, M. J.; Trucks, G. W.; Schlegel, H. B.; Scuseria, G. E.; Robb, M. A.; Cheeseman, J. R; Scalmani, G.; Barone, V.; Mennucci, B.; Petersson, G. A.; Nakatsuji, H.; Caricato, M.; Li, X.; Hratchian, H. P.; Izmaylov, A. F.; Bloino, J.; Zheng, G.; Sonnenberg, J. L.; Hada, M.; Ehara, M.; Toyota, K.; Fukuda, R.; Hasegawa, J.; Ishida, M.; Nakajima, T.; Honda, Y.; Kitao, O.; Nakai, H.; Vreven, T.; Montgomery, J. A.; Jr.; Peralta, J. E; Ogliaro, F.; Bearpark, M.; Heyd,J. J.; Brothers, E.; Kudin, K. N.; Staroverov, V. N; Kobayashi, R.; Normand, J.; Raghavachari, K.; Rendell, A.; Burant, J. C.; Iyengar, S. S.; Tomasi, J.; Cossi, M.; Rega, N.; Millam, J. M; Klene, M.; Knox, J. E.; Cross, J. B.; Bakken, V.; Adamo, C.; Jaramillo, J.; Gomperts, R.; Stratmann, R. E.; Yazyev, O.; Austin, A. J; Cammi, R.; Pomelli, C.; Ochterski, J. W.; Martin, R. L.; Morokuma, K.; Zakrzewski, V. G.; Voth, G. A.; Salvador, P.; Dannenberg, J. J.; Dapprich, S.; Daniels, A. D.; Farkas, O.; Foresman, J. B.; Ortiz, J. V.; Cioslowski, J.; Fox, D. J. *Gaussian 09, revision A.02;* Gaussian, Inc.: Wallingford: CT, 2009.
(27) Gorelsky, S. I. *AOMix: Program for Molecular Orbital Analysis;* York University, Toronto, Canada, 1997.
(28) (a) Hubbard, J. L.; Lichtenberger, D. L. *Inorg. Chem.* **1980**, *19*, 3865. (b) Fox, D. C.; Fiedler, A. T.; Halfen, H. L.; Brunold, T. C.; Haifen, J. A. *J. Am. Chem. Soc.* **2004**, *126*, 7627.
(29) Talarico, A. M.; Aiello, I.; Bellusci, A.; Crispini, A.; Ghedini, M.; Godbert, N.; Pugliese, T.; Szerb, E. *Dalton Trans.* **2010**, *39*, 1709.
(30) (a) Bleeke, J. R.; Blanchard, J. M. B.; Donnay, E. *Organometallics* **2000**, *20*, 324. (b) Gamero-Melo, P.; Cervantes-Vásquez, M.; Ramirez-Monroy, A.; Sánchez-Castro, M. E.; Paz-Sandoval, M. A. *Organometallics* **2004**, *23*, 3290. (c) Chan, K.-W.; Sau, Y.-K.; Zhang, Q.-F.; Wong, W.-Y.; Williams, I. D.; Leung, W.-H. *Eur. J. Inorg. Chem.* **2008**, 4353. (d) Gorol, M.; Roesky, H. W.; Noltemeyer, M.; Schmidt, H.-G. *Eur. J. Inorg. Chem.* **2005**, 4840.
(31) Gamero-Melo, P.; Melo-Trejo, P. A.; Cervantes-Vasquez, M.; Mendizabal-Navarro, N. P.; Paz-Michel, B.; Villar-Masetto, T. I.; Gonzalez-Fuentes, M. A.; Paz-Sandoval, M. A. *Organometallics* **2011**, *31*, 170.
(32) Paz-Michel, B. A.; González-Bravo, F. J.; Hernández-Muñoz, L. S.; Guzei, I. A.; Paz-Sandoval, M. A. *Organometallics* **2010**, *29*, 3694.
(33) (a) Xi, R.; Abe, M.; Suzuki, T.; Nishioka, T.; Isobe, K. *J. Organomet. Chem.* **1997**, *549*, 117. (b) Sugimoto, H.; Tsuge, K.; Tanaka, K. *J. Chem. Soc., Dalton Trans.* **2001**, 57. (c) Sellmann, D.; Hein, K.; Heinemann, F. W. *Inorg. Chim. Acta* **2004**, *357*, 3739. (d) Mendoza, C.; Bernès, S.; Torrens, H.; Arroyo, M. *Organometallics* **2010**, *29*, 2646.
(34) Kawamoto, T.; Takino, Y.; Sakoda, K.; Konno, T. *Chem. Lett.* **2010**, *39*, 1264.
(35) Grapperhaus, C. A.; Mullins, C. S.; Kozlowski, P. M.; Mashuta, M. S. *Inorg. Chem.* **2004**, *43*, 2859.
(36) (a) Nazeeruddin, M. K.; Wegh, R. T.; Zhou, Z.; Klein, C.; Wang, Q.; De Angelis, F.; Fantacci, S.; Grätzel, M. *Inorg. Chem.* **2006**, *45*, 9245.
(37) (a) Ballhausen, C. J. *Prog. Inorg. Chem.* **1960**, *2*, 251. (b) Creutz, C.; Newton, M. D.; Sutin, N. *J. Photochem. Photobiol., A* **1994**, *82*, 47.
(38) Gabrielsson, A.; Busby, M.; Matousek, P.; Towrie, M.; Hevia, E.; Cuesta, L.; Perez, J.; Záliš, S.; Vlček, A. *Inorg. Chem.* **2006**, *45*, 9789.
(39) (a) King, K. A.; Spellane, P. J.; Watts, R. J. *J. Am. Chem. Soc.* **1985**, *107*, 1431.
(40) Ohsawa, Y.; Sprouse, S.; King, K. A.; DeArmond, M. K.; Hanck, K. W.; Watts, R. J. *J. Phys. Chem.* **1987**, *91*, 1047.
(41) (a) Colombo, M. G.; Brunold, T. C.; Riedener, T.; Guedel, H. U.; Fortsch, M.; Buergi, H.-B. *Inorg. Chem.* **1994**, *33*, 545. (b) Hofbeck, T.; Yersin, H. *Inorg. Chem.* **2010**, *49*, 9290. (c) Colombo, M. G.; Hauser, A.; Guedel, H. U. *Inorg. Chem.* **1993**, *32*, 3088. (d) Constable, E. C.; Ertl, C. D.; Housecroft, C. E.; Zampese, J. A. *Dalton Trans.* **2014**, *43*, 5343.